

# Autoimmunity Initiates in Nonhematopoietic Cells and Progresses via Lymphocytes in an Interferon-Dependent Autoimmune Disease

Alevtina Gall,<sup>1</sup> Piper Treuting,<sup>2</sup> Keith B. Elkon,<sup>1,3</sup> Yueh-Ming Loo,<sup>1</sup> Michael Gale, Jr.,<sup>1</sup> Glen N. Barber,<sup>4</sup> and Daniel B. Stetson<sup>1,\*</sup>

<sup>1</sup>Department of Immunology

<sup>2</sup>Department of Comparative Medicine

<sup>3</sup>Division of Rheumatology

University of Washington School of Medicine, Seattle, WA 98195, USA

<sup>4</sup>Department of Medicine and Sylvester Comprehensive Cancer Center, University of Miami Miller School of Medicine, Miami, FL 33136, USA

\*Correspondence: [stetson@uw.edu](mailto:stetson@uw.edu)

DOI 10.1016/j.immuni.2011.11.018

## SUMMARY

The type I interferon (IFN) response initiated by detection of nucleic acids is important for antiviral defense but is also associated with specific autoimmune diseases. Mutations in the human 3' repair exonuclease 1 (*Trex1*) gene cause Aicardi-Goutières syndrome (AGS), an IFN-associated autoimmune disease. However, the source of the type I IFN response and the precise mechanisms of disease in AGS remain unknown. Here, we demonstrate that *Trex1* is an essential negative regulator of the STING-dependent antiviral response. We used an in vivo reporter of IFN activity in *Trex1*-deficient mice to localize the initiation of disease to nonhematopoietic cells. These IFNs drove T cell-mediated inflammation and an autoantibody response that targeted abundant, tissue-restricted autoantigens. However, B cells contributed to mortality independently of T cell-mediated tissue damage. These findings reveal a stepwise progression of autoimmune disease in *Trex1*-deficient mice, with implications for the treatment of AGS and related disorders.

## INTRODUCTION

Innate immune detection of nucleic acids is an essential component of the host response to viral infection (Barbalat et al., 2011). In vertebrates, two families of nucleic acid receptors activate the antiviral response. Toll-like receptors (TLRs) expressed by sentinel innate immune cells survey phagocytosed material for the presence of foreign nucleic acids. In contrast, intracellular nucleic acid sensors are more broadly expressed and signal a cell-intrinsic response to viral infection. In recent years, many of these innate immune sensors have been identified and characterized in great detail. They include TLR3, TLR7, and TLR8, which detect various structural features of RNA, and TLR9, which is activated by DNA. The intracellular RNA helicases RIG-I and MDA5 detect viral RNA, whereas intracellular DNA

sensing involves AIM2, DAI, IFI16, and other currently unknown receptors (reviewed in Barbalat et al., 2011). All of these receptors (with the exception of AIM2) activate expression of the type I interferon (IFN) family of cytokines, which act to block viral replication within infected cells and facilitate adaptive immune responses to viral antigens (Stark et al., 1998; Stetson and Medzhitov, 2006b).

The IFN response triggered by nucleic acid receptors is important for protection against infection, but it must be carefully regulated to prevent inappropriate activation by endogenous DNA and RNA. Recent studies have found that chronic activation of these antiviral sensors can cause a number of severe autoimmune diseases (Banchereau and Pascual, 2006; Theofilopoulos et al., 2005). In normal settings, this chronic activation is prevented by regulating the expression and compartmentalization of the sensors themselves (Barton and Kagan, 2009) and by the activity of RNA and DNA nucleases that metabolize the ligands for the receptors (Nagata et al., 2010). Thus, the imperfect ability of innate immune receptors to distinguish between endogenous and foreign nucleic acids is enabled in large part by the activities of accessory proteins.

Recent advances have established central roles for nucleic acid-sensing TLRs and type I IFNs in a number of severe autoimmune diseases, including systemic lupus erythematosus (SLE) and psoriasis (Barrat et al., 2005; Christensen et al., 2006; Lande et al., 2007; Leadbetter et al., 2002). In addition, chronic activation of cell-intrinsic antiviral responses can also cause autoimmunity. Specifically, we identified 3' repair exonuclease 1 (*Trex1*) as an essential negative regulator of the antiviral response triggered by detection of intracellular DNA (Stetson et al., 2008). In *Trex1*-deficient mice, endogenous DNA substrates accumulate and trigger a lethal, type I IFN-dependent autoimmune disease. These *Trex1* substrates include reverse-transcribed DNA derived from endogenous retroelements (Stetson et al., 2008), and *Trex1* can also metabolize human immunodeficiency virus (HIV) cDNA within infected cells (Yan et al., 2010), suggesting a key role for this pathway in antiretroviral defense and an important contribution of nucleic acids derived from endogenous retroelements to autoimmune disease.

Interestingly, detection of intracellular DNA can activate two distinct antiviral responses in cells. One pathway, called the interferon-stimulatory DNA (ISD) response (Stetson and

Medzhitov, 2006a), is activated by natural DNA containing all four bases and triggers type I interferon production through the adaptor protein STING (Ishikawa et al., 2009). In contrast, the synthetic DNA polymer poly(dA:dT) can activate the STING-dependent pathway and can also be transcribed by cellular RNA polymerase III into a triphosphate RNA ligand that activates the RIG-I-MAVS pathway (Ablasser et al., 2009; Chiu et al., 2009; Ishii et al., 2006). Thus, although it is clear that *Trex1* negatively regulates the DNA-activated antiviral response, it remains unknown whether *Trex1* regulates the ISD pathway, the Pol-III pathway, or both.

Loss-of-function mutations in the human *Trex1* gene cause Aicardi-Goutières syndrome (AGS), a rare and severe autoimmune disease that presents in infancy and mimics the features of congenital viral infection (Crow et al., 2006). AGS is characterized by elevated type I IFNs, brain inflammation, and profound psychomotor retardation, with a mortality rate approaching 35% by 15 years of age (Rice et al., 2007b). Currently, there are no effective therapies for AGS, and the precise mechanisms of disease remain incompletely defined.

Since the seminal identification of *Trex1* mutations in AGS, dozens of distinct mutations within the human *Trex1* open reading frame have been discovered in the context of several disease phenotypes, including chilblain lupus and SLE (de Vries et al., 2010; Lee-Kirsch et al., 2007; Namjou et al., 2011; Rice et al., 2007a). Remarkably, some of these mutations are identical to those that cause AGS. Although the precise functional consequences of many of these rare, lupus-associated *Trex1* mutations remain unknown, the genetic association of *Trex1* mutations with SLE is the strongest of any single gene identified to date (Harley et al., 2009). Together, these studies clearly link *Trex1* and the cell-intrinsic antiviral response to DNA to a number of IFN-associated human autoimmune disorders.

*Trex1*-deficient (*Trex1*<sup>-/-</sup>) mice, with a highly penetrant and severe phenotype, are an excellent model for exploring the mechanistic basis of disease, with direct relevance to human AGS and SLE. These mice are particularly amenable to genetic dissection of autoimmunity through crosses with mice deficient in key components of innate and adaptive immunity. For example, we found that *Trex1*<sup>-/-</sup> mice lacking interferon regulatory factor 3 (IRF3), the type I IFN receptor (Irfar1), or RAG2 are all completely protected from autoimmune pathology and mortality (Stetson et al., 2008). However, a number of important questions remain: which DNA-activated antiviral response does *Trex1* regulate? Which cells initiate the disease, where, and when? How does chronic activation of the ISD pathway lead to lymphocyte-dependent autoimmunity? And what are the specific contributions of lymphocytes to disease?

Here, we present a detailed characterization of the development of disease in *Trex1*-deficient mice, from its earliest initiation to organ-specific autoimmune pathology. We establish *Trex1* as a unique regulator of the STING-dependent ISD pathway. We employ an in vivo reporter of the type I IFN response to localize the initiation of disease and we determine how these IFNs drive the autoreactive lymphocyte response. We show that both T cells and B cells contribute to disease through distinct mechanisms. Together, these findings provide new insight into the progression of IFN-mediated autoimmunity, with implications for the human diseases caused by chronic activation of the ISD pathway.

## RESULTS

### *Trex1*-Deficient Mice Develop Specific Multiorgan Inflammation

*Trex1*-deficient mice on a C57BL/6 background develop a severe autoimmune disease, with a median life span of 10 weeks in our colony (Morita et al., 2004; Stetson et al., 2008). Inflammatory myocarditis is evident in all *Trex1*<sup>-/-</sup> mice, but the extent to which other tissues are affected has not been examined. We performed a thorough histological analysis of all major tissues and organs in *Trex1*-deficient mice (Figure 1). In the heart, we found coalescing regions of lymphohistiocytic, degenerative, and, in severe cases, fibrosing myocarditis. This myocarditis was most prominent near the endocardial surface. We also found that *Trex1*-deficient mice reproducibly developed profound inflammation in skeletal muscle, tongue, skin, and the glandular stomach. Similar to the heart, the skeletal muscles and tongue had lymphohistiocytic and degenerative to fibrosing myositis. In the haired skin of the muzzle, there was also mild to moderate lymphohistiocytic dermatitis, perifolliculitis, and myositis. Finally, the glandular stomach had chronic lymphoid aggregates within the mucosa and moderate proliferative gastritis. Importantly, numerous organs were not affected by *Trex1* deficiency, including brain, colon, small intestine, pancreas, lung, and liver (Figure 1 and unpublished data). Together, these findings reveal that the autoimmune disease in *Trex1*-deficient mice targets multiple, specific organs.

### *Trex1* Is a Specific Negative Regulator of STING-Dependent Signaling

The multiorgan autoimmune disease in *Trex1*-deficient mice requires IRF3 and type I IFNs (Stetson et al., 2008), and extranuclear DNA accumulates in *Trex1*-deficient cells (Stetson et al., 2008; Yang et al., 2007). This accumulated DNA could conceivably activate two distinct antiviral responses: the ISD-STING pathway (Ishikawa et al., 2009) or the Pol-III-RIG-I-MAVS pathway (Ablasser et al., 2009; Chiu et al., 2009). To determine which of these two DNA-activated antiviral responses is regulated by *Trex1*, we crossed *Trex1*<sup>-/-</sup> mice to *Mavs*<sup>-/-</sup> mice and to *Tmem173*<sup>-/-</sup> (STING-deficient) mice. We found that *Trex1*<sup>-/-</sup> *Mavs*<sup>-/-</sup> mice developed identical autoimmune disease and succumbed with identical kinetics when compared to *Trex1*<sup>-/-</sup> mice (Figures 2A–2C). In contrast, *Trex1*<sup>-/-</sup> *Tmem173*<sup>-/-</sup> mice were completely rescued from mortality and autoimmune tissue destruction (Figures 2A–2C). *Trex1*<sup>-/-</sup> mice that were heterozygous for *Tmem173* were also protected from mortality (Figure 2A), even more so than *Trex1*<sup>-/-</sup> *Irf3*<sup>+/-</sup> mice (Stetson et al., 2008). These two crosses formally establish *Trex1* as a specific and essential negative regulator of the STING-dependent ISD pathway and suggest a prominent role for STING in AGS and related human diseases. Moreover, we uncover a dramatic phenotypic consequence of STING haploinsufficiency—protection from autoimmune disease—that may offer an evolutionary explanation for the recently reported existence of hypomorphic *TMEM173* alleles in the human population (Jin et al., 2011).

### Tracking the Origins of Type I Interferon-Mediated Disease In Vivo

AGS in humans is strongly associated with an elevated type I IFN response (Lebon et al., 1988), and *Trex1*-deficient mice lacking

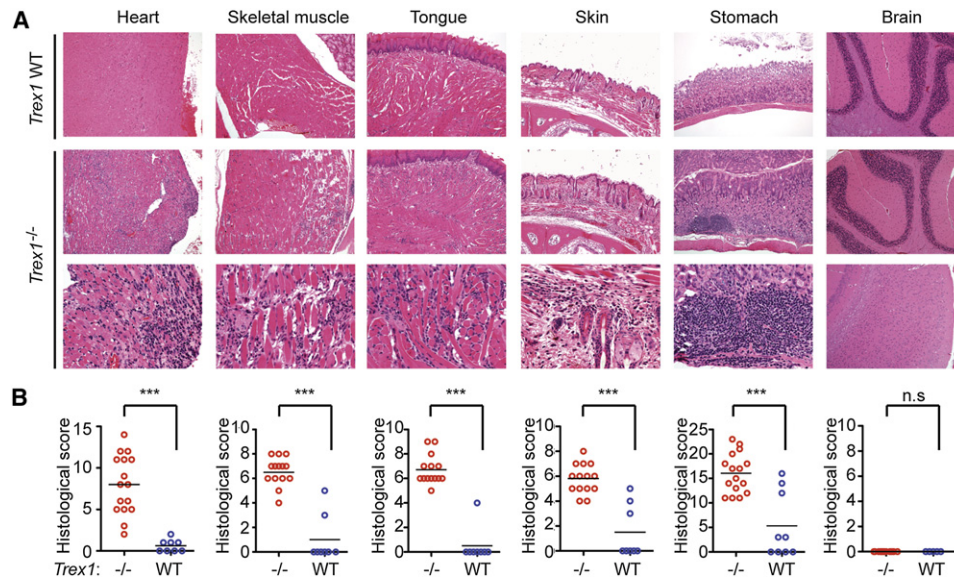


**Figure 1. *Trex1*<sup>-/-</sup> Mice Develop Specific Multiorgan Inflammation**

(A) Representative hematoxylin and eosin-stained (H&E) tissue sections from *Trex1* WT (top row) and *Trex1*<sup>-/-</sup> (bottom two rows) mice. Skeletal muscle samples were taken from the masseter. Brain sections are from the cerebellum (top panels) and the neocortex (lower panel). Original magnifications: top two rows 10 $\times$ ; bottom row 20 $\times$  except for neocortex, 10 $\times$ .

(B) Blinded analysis of indicated tissues from *Trex1*<sup>-/-</sup> (red) or WT (blue) mice. Data are represented as histological scores from individual animals and the mean (horizontal line) of experimental groups. Statistical analysis was performed with a two-tailed, unpaired Student's t test. n.s. = not statistically significant ( $p > 0.05$ ); \*\*\* $p \leq 0.0005$ .

the type I IFN receptor (*Ifnar1*) are completely protected from tissue damage and mortality (Stetson et al., 2008). Given the absolute requirement for STING-dependent type I IFNs in this mouse model, we performed a simple genetic cross to track the IFN response in vivo during disease initiation and progression. We bred *Trex1*<sup>+/-</sup> mice carrying an Mx1-Cre transgene (Kühn et al., 1995) to *Trex1*<sup>-/-</sup>*Rag2*<sup>-/-</sup> mice homozygous for the Cre-activated Rosa26-YFP reporter allele (Srinivas et al., 2001), thereby generating *Trex1*<sup>+/-</sup> controls and *Trex1*<sup>-/-</sup> mice with an in vivo reporter of IFN activity (Figure 3A). Specifically, IFN signaling activates expression of the IFN-inducible Mx-Cre transgene, which then excises the LoxP-flanked “stop cassette” in the Rosa26-YFP reporter allele, thus turning any IFN-responsive cell brightly and permanently YFP<sup>+</sup>. We examined peripheral blood from *Trex1*<sup>-/-</sup> and control reporter mice and found that 1 day after birth, 20% of circulating leukocytes were YFP<sup>+</sup> in *Trex1*-deficient reporter mice, compared with only 3% YFP<sup>+</sup> cells in control mice (Figures 3A and 3B). By day 3, the frequency of YFP<sup>+</sup> cells in *Trex1*<sup>-/-</sup> reporter mice increased to more than 60% and then further increased to a maximum of almost 80% by 4 weeks of age. We observed a similar early emergence and accumulation of YFP<sup>+</sup> cells in *Trex1*<sup>-/-</sup> reporter mice on a *Rag2*<sup>-/-</sup> background, which demonstrated that the IFN response was independent of lymphocytes (Figure 3A, right column). We confirmed these findings by measuring expression of ISG15, an interferon-inducible gene, in whole embryos of plain *Trex1*<sup>-/-</sup> mice and controls. We found that at E14 and E17, ISG15 expression was elevated in *Trex1*-deficient mice compared to controls (Figure 3C). Thus, the IFN response that drives disease in *Trex1*-deficient mice develops in utero and

precedes lymphocyte-dependent inflammation and autoimmune tissue damage.

Based on the detection of an early systemic type I IFN response in circulating leukocytes in *Trex1*-deficient reporter mice, we examined heart tissue by immunofluorescence microscopy to track the in situ emergence of this response within an organ that is strongly affected by the autoimmune disease. By day 3 after birth, we reproducibly detected (in three out of four mice examined) a localized focus of YFP<sup>+</sup> cells near the endocardial surface of the apex of the heart in *Trex1*-deficient reporter mice (Figure 3D). The distribution of YFP<sup>+</sup> cells became more widespread by day 5, but remained concentrated near the endocardial surface (Figure 3D). By day 28, we observed a dramatic expansion of reporter fluorescence with the most robust signal along the entire endocardial surface of the heart, which correlated strongly with the site of the most extensive inflammation (Figures 3D and 1A). These in situ data, while qualitative, reveal a number of important insights into the origins of disease in *Trex1*-deficient mice. First, the initial emergence of a detectable IFN response in the heart occurs shortly after birth in a geographically restricted subset of cardiac cells. Second, this IFN response spreads rapidly but remains localized near the endocardial surface, suggesting a process that drives the IFN response specifically in these cells but not other, nearby cells. Finally, the spatial overlap between the early IFN reporter signal and the later inflammatory infiltrate suggests a causal relationship between the site of the initial, tissue-restricted IFN response and the site of subsequent autoimmune inflammation within the target tissue.

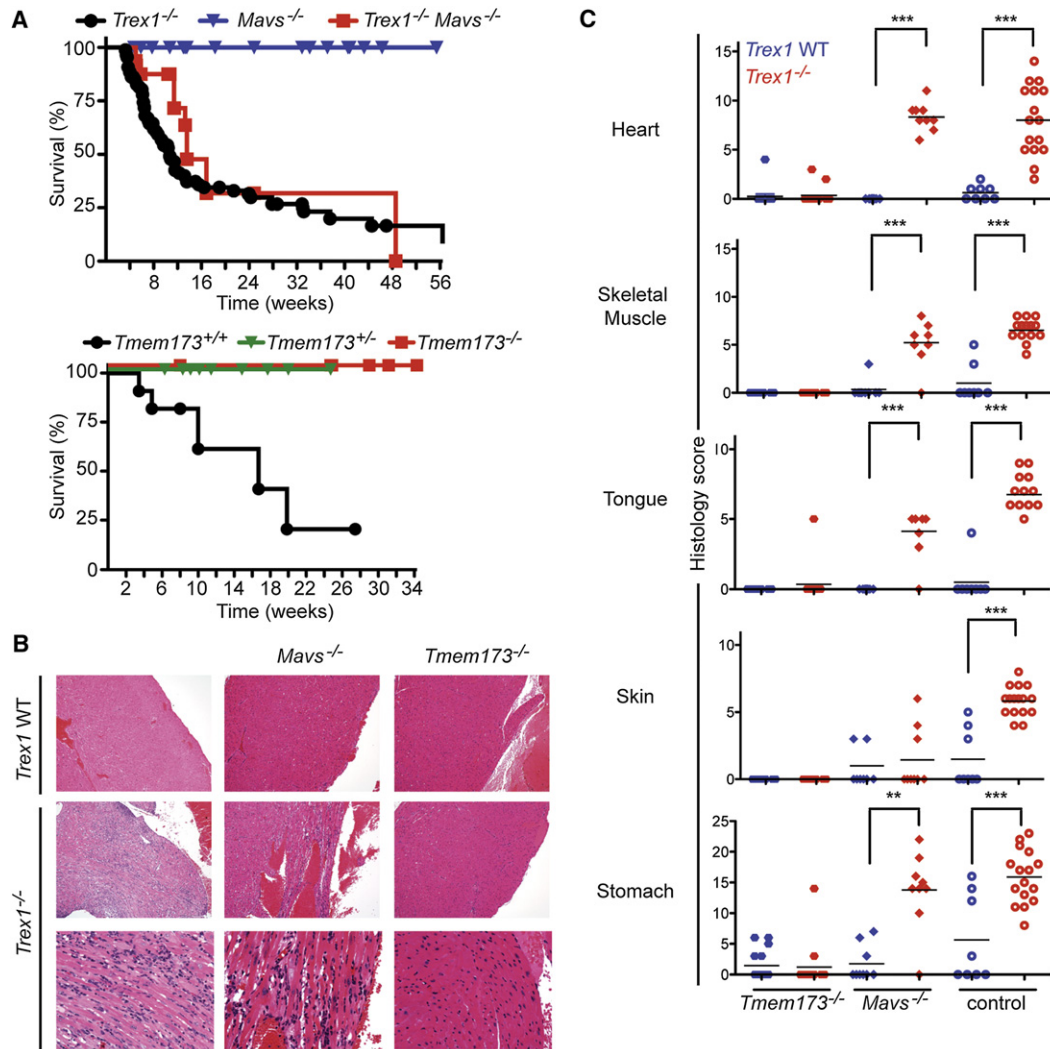


### Figure 2. *Trex1* Is a Specific Negative Regulator of STING-Dependent Signaling

(A) Survival curves of *Trex1*<sup>-/-</sup> mice, *Mavs*<sup>-/-</sup> mice, and *Trex1*<sup>-/-</sup> *Mavs*<sup>-/-</sup> mice. The *Mavs*<sup>-/-</sup> mice were generated on a pure C57BL/6 background, so the plain *Trex1*<sup>-/-</sup> controls include mice generated from other contemporary crosses within this background. The *Tmem173*<sup>-/-</sup> mice were on a mixed C57BL/6:129 background, and plain *Trex1*<sup>-/-</sup> mice generated from intercrossing *Trex1*<sup>+/-</sup> *Tmem173*<sup>+/+</sup> mice are shown as controls.

(B) Representative H&E-stained heart tissue sections from mice of the indicated genotypes. The original magnification in the top row is 10x and in the bottom two rows is 20x.

(C) Blinded analysis of the indicated tissues of *Trex1*<sup>-/-</sup> mice crossed to *Tmem173*<sup>-/-</sup> and *Mavs*<sup>-/-</sup> mice. Plain *Trex1*<sup>-/-</sup> mice and controls are the same as in Figure 1B and are presented for direct comparison to the other genotypes. For these and all other histological analyses presented below, statistical analysis was performed with a two-tailed, one-way ANOVA with Tukey's multiple comparison posttest. \*p < 0.05, \*\*p ≤ 0.005, \*\*\*p ≤ 0.0005.

### Nonhematopoietic Cells Initiate Autoimmune Disease in *Trex1*-Deficient Mice

The early emergence of a type I IFN response within the endocardial region of *Trex1*-deficient hearts suggested that a tissue-restricted IFN response might initiate the disease process. To test this possibility, we performed a series of bone marrow chimeras to establish tissue-specific requirements for *Trex1* deficiency in the progression of autoimmune inflammation. We used *Trex1*<sup>+/-</sup> or *Trex1*<sup>-/-</sup> mice on a *Rag2*<sup>-/-</sup> background as recipients; *Trex1*<sup>+/-</sup> *Rag2*<sup>-/-</sup> mice are completely rescued from autoimmune pathology and mortality but still initiate a type I IFN response (Figure 3A; Stetson et al., 2008), thus allowing us

to examine the effects of hematopoietic reconstitution without potentially confounding our results with preexisting inflammation in the mutant recipients. We reconstituted irradiated *Rag2*<sup>-/-</sup> controls or *Trex1*<sup>-/-</sup> *Rag2*<sup>-/-</sup> mice with either wild-type (WT) bone marrow or *Ifnar1*<sup>-/-</sup> bone marrow. All of the *Trex1*<sup>-/-</sup> *Rag2*<sup>-/-</sup> mice that received WT bone marrow exhibited dramatic morbidity and mortality beginning 6 weeks after reconstitution (Figure 4A). In contrast, all of the *Trex1*<sup>-/-</sup> *Rag2*<sup>-/-</sup> mice reconstituted with *Ifnar1*<sup>-/-</sup> bone marrow remained alive and healthy. *Rag2*<sup>-/-</sup> control recipients survived after reconstitution with either WT or *Ifnar1*<sup>-/-</sup> bone marrow. Histological analysis of hearts by the same criteria described in Figure 1 revealed a

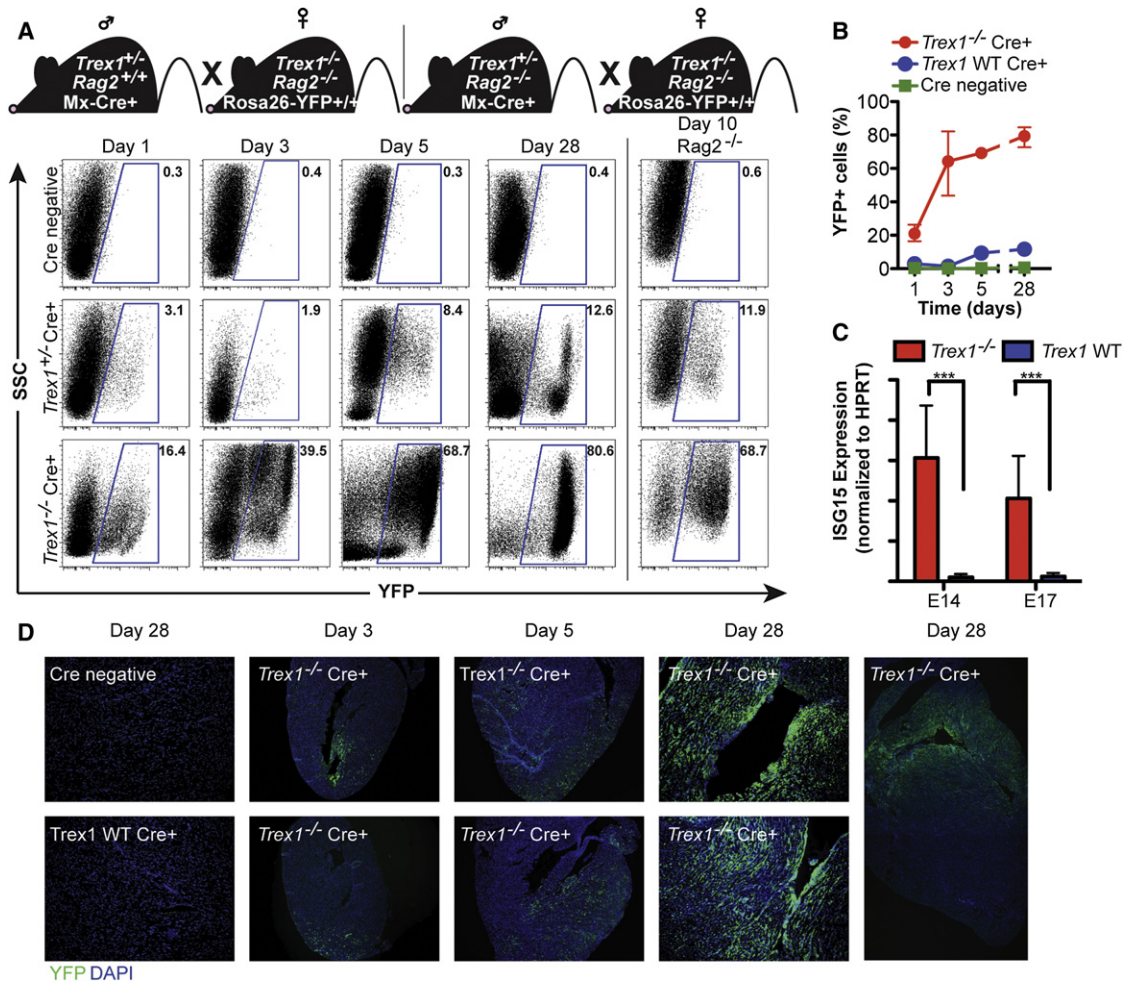


**Figure 3. Origins of the Type I IFN Response in *Trex1*-Deficient Mice**

(A) Representative flow cytometry plots of YFP expression in peripheral blood of  $Trex1^{-/-} Rag2^{+/-}$  Rosa26-YFP<sup>R/WT</sup> Mx-Cre<sup>+</sup> or  $Trex1^{-/-} Rag2^{-/-}$  Rosa26-YFP<sup>R/WT</sup> Mx-Cre<sup>+</sup> and control mice of indicated ages.

(B) Percentage of YFP<sup>+</sup> cells from  $Trex1^{-/-} Rag2^{+/-}$  Rosa26-YFP<sup>R/WT</sup> Mx-Cre<sup>+</sup> and control mice of indicated ages. Data are represented as means of percentages (n ≤ 7) and range.

(C)  $Trex1^{-/-}$  and control embryos of the indicated gestational age were analyzed by quantitative RT-PCR for expression of ISG15. Data are from three to six littermates per genotype and are presented as the ratio of ISG15 to HPRT. \*\*\*p ≤ 0.0005.

(D) Longitudinal analysis of YFP expression in heart tissue sections from  $Trex1^{-/-} Rag2^{+/-}$  Rosa26-YFP<sup>R/WT</sup> Mx-Cre<sup>+</sup> and control mice of the indicated ages. Sections were stained with anti-GFP rabbit polyclonal antibody followed by tyramide amplification (green fluorescence) and counterstained with DAPI (blue).

radiation-induced heart inflammation that was present in all mice, regardless of the genotype of the recipient or the source of the bone marrow (Figure 4B). Within the background of this radiation-induced inflammation, we observed a slight but statistically insignificant increase in inflammation in the  $Trex1^{-/-} Rag2^{-/-}$  mice reconstituted with WT bone marrow (Figure 4B).

We next created mixed bone marrow chimeras in which we reconstituted  $Rag2^{-/-}$  mice or  $Trex1^{-/-} Rag2^{-/-}$  mice with a ~2:1 mixture of *Ifnar1*<sup>-/-</sup> (CD45.1):WT (CD45.2) bone marrow.  $Trex1^{-/-} Rag2^{-/-}$  mice that received the mixed bone marrow succumbed to disease with similar kinetics to those that received only WT bone marrow (Figure 4C), whereas the  $Rag2^{-/-}$  recipients remained healthy. We examined the ratio of WT:*Ifnar1*<sup>-/-</sup> CD4 T cells in the blood, spleens, and hearts of

a cohort of recipient mice euthanized 6 weeks postreconstitution. The  $Rag2^{-/-}$  control recipients maintained a ratio of WT:*Ifnar1*<sup>-/-</sup> cells in all three tissues that was identical to the input ratio. In contrast, we observed a strong bias toward WT CD4 T cells in the  $Trex1^{-/-} Rag2^{-/-}$  recipients that was most dramatic in the heart tissue (Figures 4D and 4E). This strong WT bias was also present in CD8 T cells and in B cells, again most prominently among the cells recovered from the heart (data not shown). Taken together with the in situ analysis of the IFN response in the reporter mice, these data define tissue-specific requirements for *Trex1* deficiency and type I IFNs in the initiation and progression of disease. First, *Trex1* deficiency in nonhematopoietic cells is sufficient to drive disease, even in the presence of a WT hematopoietic system. Second, *Trex1* deficiency in hematopoietic cells, specifically lymphocytes, is

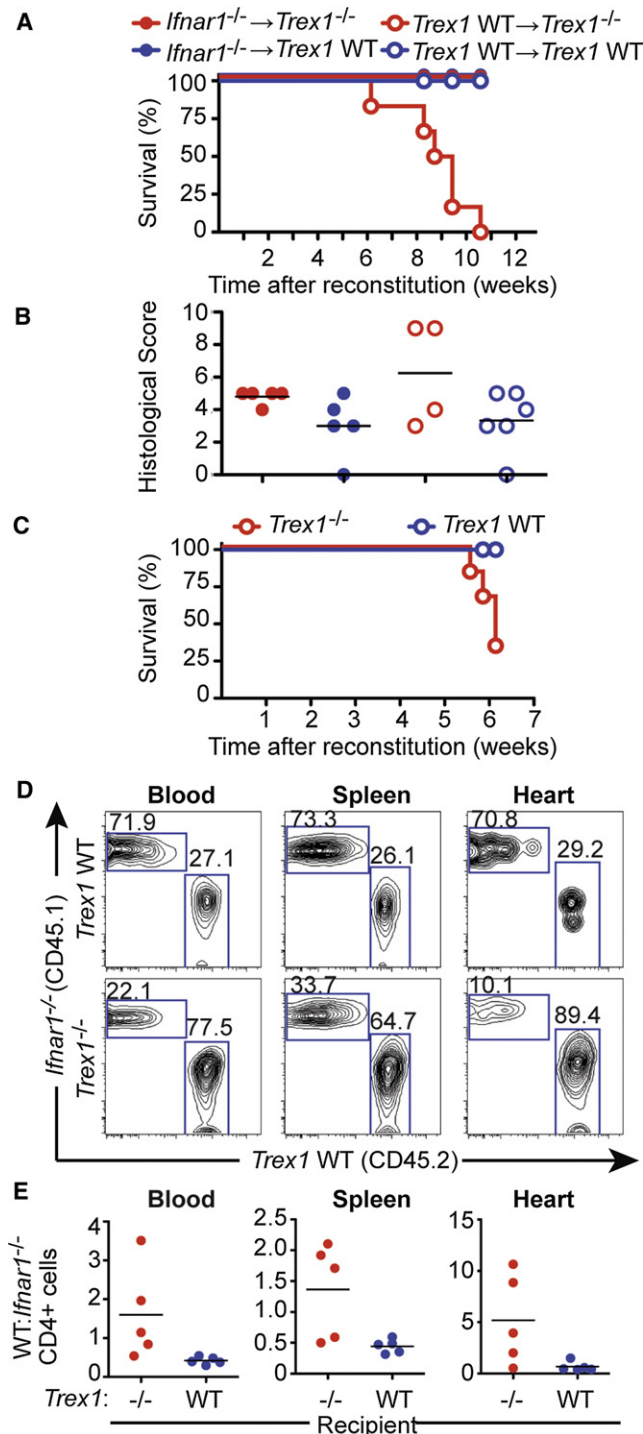


**Figure 4. Nonhematopoietic Cells Initiate Disease in Trex1-Deficient Mice**

(A) Survival curves of female *Trex1*<sup>-/-</sup>*Rag2*<sup>-/-</sup> or *Rag2*<sup>-/-</sup> mice reconstituted with either *Ifnar1*<sup>-/-</sup> or WT bone marrow. Graph shows results from one out of two independent experiments, each with five mice per group.  
 (B) Histological scores of hearts from *Trex1*<sup>-/-</sup> or WT female mice reconstituted with either *Ifnar1*<sup>-/-</sup> or WT bone marrow.  
 (C) Percent survival of *Trex1*<sup>-/-</sup>*Rag2*<sup>-/-</sup> or *Rag2*<sup>-/-</sup> female mice (n = 5 per group) reconstituted with a ~2:1 ratio of *Ifnar1*<sup>-/-</sup> (CD45.1):WT (CD45.2) bone marrow. Graph is representative of one out of two independent experiments.

not required for the autoimmune response. Third, type I IFN receptor signaling in hematopoietic cells is required to sense the IFNs produced by the initiating cells, and this signaling favors the expansion and/or recruitment of autoreactive lymphocytes to the target organ. This IFN-dependent lymphocyte expansion is identical to what has been reported for T cell responses to viral infection (Kolumam et al., 2005), suggesting that similar mechanisms mediate both protective and autoimmune lymphocyte responses triggered by innate immune detection of nucleic acids.

**T Cells and B Cells Drive Inflammation and Mortality in Trex1-Deficient Mice**

The IFN-dependent appearance of lymphocytes in the hearts of *Trex1*-deficient recipients, together with our previous observation that lymphocytes are required for inflammation and mortality (Stetson et al., 2008), led us to explore the individual contributions of  $\alpha\beta$  T cells and B cells to the autoimmune inflammation in *Trex1*<sup>-/-</sup> mice. We generated *Trex1*<sup>-/-</sup>*Tcra*<sup>-/-</sup> mice and *Trex1*<sup>-/-</sup>*Ighm*<sup>-/-</sup> mice and performed an extensive survival and histological analysis of these mice and controls, compared with plain *Trex1*<sup>-/-</sup> mice. *Tcra*-deficient mice develop an inflammatory bowel disease that is caused by a population of TCR $\beta$ <sup>+</sup> lymphocytes that respond to environmental *Helicobacter* antigens (Takahashi et al., 1999). Indeed, we found that the plain *Tcra*<sup>-/-</sup> mice in our colony suffered from increased mortality associated with severe colitis (Figures 5A and 5E). Remarkably, *Trex1*<sup>-/-</sup>*Tcra*<sup>-/-</sup> mice were rescued from mortality compared with plain *Trex1*<sup>-/-</sup> mice, and even compared with plain *Tcra*<sup>-/-</sup> mice (Figure 5A). Thus,  $\alpha\beta$  T cells are essential for the mortality caused by *Trex1* deficiency.

We found that *Trex1*<sup>-/-</sup>*Ighm*<sup>-/-</sup> mice that lack B cells were dramatically rescued from mortality, with a median lifespan that was more than seven times longer than plain *Trex1*<sup>-/-</sup> mice (73 weeks versus 10 weeks; Figure 5A). However, after 1 year, survival of *Trex1*<sup>-/-</sup>*Ighm*<sup>-/-</sup> mice declined steadily compared to *Ighm*<sup>-/-</sup> littermate controls, suggesting that although B cells clearly play a central role in the rapid mortality caused by *Trex1* deficiency, *Trex1*-deficient mice lacking B cells are not completely protected from disease.

We performed a thorough histological analysis of the affected tissues of *Trex1*<sup>-/-</sup> mice, *Trex1*<sup>-/-</sup>*Tcra*<sup>-/-</sup> mice, and *Trex1*<sup>-/-</sup>*Ighm*<sup>-/-</sup> mice, along with *Trex1* WT controls from each cross. Remarkably, we found that  $\alpha\beta$  T cells were absolutely required for inflammation and tissue damage associated with *Trex1* deficiency, but B cells were largely dispensable for this inflammation. Representative heart tissue sections in Figure 5B and histological scores in Figure 5C revealed that *Trex1*<sup>-/-</sup>*Tcra*<sup>-/-</sup> mice were completely protected from inflammation, but *Trex1*<sup>-/-</sup>*Ighm*<sup>-/-</sup> mice developed extensive heart inflammation that was statistically indistinguishable from that which developed in plain *Trex1*<sup>-/-</sup> mice. In the other organs affected by *Trex1* deficiency, we found that *Trex1*<sup>-/-</sup>*Tcra*<sup>-/-</sup> mice were

(D) Representative flow cytometry plots of CD45.1 (*Ifnar1*<sup>-/-</sup>) and CD45.2 (WT) expression by CD4<sup>+</sup> cells in the indicated tissues of mixed bone marrow recipients.  
 (E) The ratio of WT:*Ifnar1*<sup>-/-</sup> CD4 T cells was calculated for the indicated organs. We obtained identical results when examining CD8 T cells and B cells.

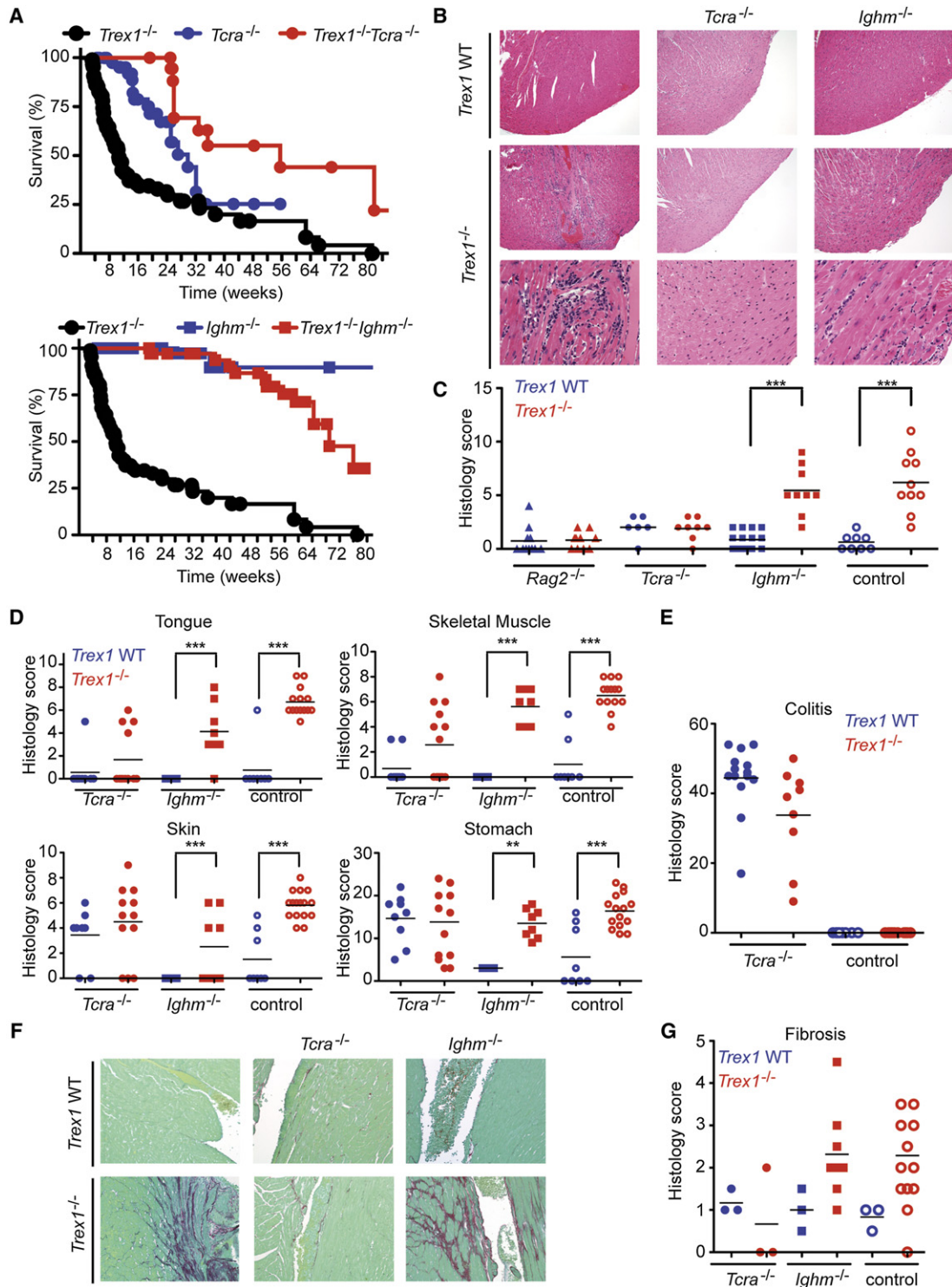


**Figure 5. Contributions of  $\alpha\beta$  T Cells and B Cells to Autoimmunity in *Trex1*<sup>-/-</sup> Mice**

(A) Survival curves for mice of indicated *Trex1*/*Tcr* (top) and *Trex1*/*Ighm* (bottom) genotypes. Median life spans of each *Trex1*<sup>-/-</sup> genotype are as follows. *Trex1*<sup>-/-</sup>, 10 weeks; *Trex1*<sup>-/-</sup>*Tcr*<sup>-/-</sup>, 56 weeks ( $p < 0.0001$ ); *Trex1*<sup>-/-</sup>*Ighm*<sup>-/-</sup>, 73 weeks ( $p < 0.0001$ ). Statistical analysis was performed with a Log-rank (Mantel-Cox) test. All mice were on a C57BL/6 background.

(B) Representative H&E-stained sections of heart apex from mice of the indicated genotypes.

(C) Blinded analysis of the endocardial region in *Trex1*<sup>-/-</sup> (red) or *Trex1* WT (blue) mice of indicated *Rag2*, *Tcr*, or *Ighm* genotype, scored as in Figure 1B. \*\*\* $p \leq 0.0005$ .

(D) Blinded analysis of tissues from *Trex1*<sup>-/-</sup> (red) or *Trex1* WT (blue) mice of indicated *Tcr* or *Ighm* genotype. \* $p < 0.05$ , \*\* $p \leq 0.005$ , \*\*\* $p \leq 0.0005$ .

indistinguishable from plain *Tcra*<sup>-/-</sup> littermates, although both *Tcra*<sup>-/-</sup> and *Trex1*<sup>-/-</sup>*Tcra*<sup>-/-</sup> mice had elevated inflammation in skeletal muscle, skin, and stomach (Figure 5D). Importantly, examination of multiple tissues allowed us to separate the effects of *Tcra* deficiency from the effects of *Trex1* deficiency, most notably in the tongue and heart, where we found no evidence of any inflammation in *Trex1*<sup>-/-</sup>*Tcra*<sup>-/-</sup> mice (Figures 5D and 5E). Thus, we conclude that the increased mortality in *Trex1*<sup>-/-</sup>*Tcra*<sup>-/-</sup> mice is due to the inflammatory bowel disease caused by *Tcra* deficiency, not the autoimmune disease caused by *Trex1* deficiency. In contrast, every tissue that exhibited autoimmune pathology in plain *Trex1*<sup>-/-</sup> mice showed similar inflammatory infiltrates in *Trex1*<sup>-/-</sup>*Ighm*<sup>-/-</sup> mice (Figure 5D), demonstrating that B cells are dispensable for autoimmune inflammation in this model.

We next tested whether differential development of fibrotic damage could explain the dramatic rescue of *Trex1*<sup>-/-</sup>*Ighm*<sup>-/-</sup> mice from mortality without amelioration of inflammation. We stained heart tissue sections with picrosirius red, which detects collagen, and found that both *Trex1*<sup>-/-</sup> mice and *Trex1*<sup>-/-</sup>*Ighm*<sup>-/-</sup> mice developed fibrosis that was most extensive near the endocardial surface, but *Trex1*<sup>-/-</sup>*Tcra*<sup>-/-</sup> mice were completely protected from fibrosis (Figures 5F and 5G). Together, these data demonstrate that the inflammation and fibrosis in *Trex1*<sup>-/-</sup> mice absolutely requires  $\alpha\beta$  T cells but is largely independent of B cells. However, B cells dramatically accelerate mortality in *Trex1*<sup>-/-</sup> mice, suggesting an uncoupling of T cell-dependent inflammation from B cell-dependent processes that may drive end-stage tissue damage.

### T Cell-Dependent Autoantibody Specificities in *Trex1*-Deficient Mice

We previously showed that *Trex1*<sup>-/-</sup> mice develop a type I IFN-dependent autoantibody response that targets heart tissue (Stetson et al., 2008). Based on the contribution of B cells to mortality in *Trex1*-deficient mice described above and the strong genetic association in humans between rare *Trex1* mutations and SLE, we characterized the specificity of this autoantibody response. We found that *Trex1*<sup>-/-</sup> mice developed anti-nuclear autoantibodies (ANA), progressive IgG deposition in kidney glomeruli, and kidney inflammation, three hallmark features of lupus (Figures 6A–6C; Figure S1 available online). However, we did not find significantly elevated levels of antichromatin IgG or anti-dsDNA autoantibodies in *Trex1*<sup>-/-</sup> mice (Figure S1), suggesting that dsDNA reactivity was not the source of the ANA signal.

We investigated the contributions of T and B cells to these lupus-like features by performing a comparative analysis of kidney pathology in *Trex1*<sup>-/-</sup>*Tcra*<sup>-/-</sup> and *Trex1*<sup>-/-</sup>*Ighm*<sup>-/-</sup> mice. Similar to all other affected tissues in *Trex1*<sup>-/-</sup> mice, we found extensive interstitial inflammation in *Trex1*<sup>-/-</sup> kidneys that was most prominent in perivascular areas (Figures 6C and 6D). This interstitial kidney inflammation required T cells but

not B cells (Figure 6C). We also observed mild membranoproliferative glomerulonephritis in *Trex1*-deficient kidneys, including hypersegmentation, expanded mesangial matrix, and increased cellularity with immune cell infiltrates (Figures 6C and 6D). Interestingly, and consistent with a causal role for immune complexes in glomerular damage, the glomeruli of *Trex1*<sup>-/-</sup>*Ighm*<sup>-/-</sup> mice were devoid of this inflammation (Figures 6C and 6D). Thus, *Trex1*-deficient mice develop some of the cardinal features of lupus, which provides mechanistic support for the strong genetic association between *TREX1* mutations and SLE in humans (Lee-Kirsch et al., 2007; Namjou et al., 2011). Moreover, we genetically separate interstitial kidney inflammation from glomerulonephritis by showing that the former requires T cells and the latter requires B cells.

We next characterized the targets of the tissue-specific autoantibody response by immunoprecipitating autoantigens from heart extracts with sera from *Trex1*<sup>-/-</sup> mice. We reproducibly recovered a number of proteins by using *Trex1*<sup>-/-</sup> sera but not control sera, two of which were identical in mass to the strongest autoantibody signals observed by protein immunoblotting of heart extracts with *Trex1*<sup>-/-</sup> sera (Figure 6E). We identified these autoantigens by mass spectrometry as cardiac myosin (Myh6) and junctophilin-2 (Jph2; Figure 6E). We confirmed the mass spectrometry data with protein immunoblot of heart immunoprecipitates by using antisera specific for Myh6 and Jph2 and found that we immunoprecipitated Myh6 and Jph2 with multiple serum samples from *Trex1*<sup>-/-</sup> mice but not from WT littermate controls (Figure 6F). Thus, *Trex1*-deficient mice reproducibly develop autoantibodies to two abundant, heart-specific, cytosolic proteins.

We tested the contribution of  $\alpha\beta$  T cells to the heart-specific autoantibody response in *Trex1*<sup>-/-</sup> mice. Sera from *Trex1*<sup>-/-</sup> mice showed strong IgG autoreactivity by protein immunoblot with extracts from both *Rag2*<sup>-/-</sup> and *Trex1*<sup>-/-</sup>*Rag2*<sup>-/-</sup> hearts. In contrast, these autoantibodies were absent in *Trex1*<sup>-/-</sup>*Tcra*<sup>-/-</sup> mice, demonstrating that the autoantibody response in *Trex1*<sup>-/-</sup> mice is T cell dependent (Figure 6G).

## DISCUSSION

Type I IFNs are associated with a number of autoimmune diseases in humans, including AGS and SLE. We describe here a detailed characterization of the origins and progression of the type I interferon-mediated autoimmune disease in a mouse model of AGS. We show that STING (Tmem173) is essential for disease in *Trex1*-deficient mice, thus formally establishing a role for the STING-dependent ISD pathway in autoimmune diseases associated with *Trex1* mutations. We identify the earliest sites of IFN production and show that these IFNs act on hematopoietic cells to enable the autoimmune response. We delineate the relative contributions of T and B cells to disease and unexpectedly reveal a prominent role for B cells that is independent of T cell-mediated inflammation and fibrotic damage.

(E) Colon sections from *Trex1*<sup>-/-</sup> (red) or *Trex1* WT (blue) mice of indicated *Tcra* genotype were graded for inflammation, mucosal changes, dysplasia, and extent of pathology.

(F) Examples of picrosirius red/fast green-stained sections of left ventricle (endocardial region) to highlight collagen (fibrosis = red staining).

(G) Endocardial and epicardial regions of the heart from *Trex1*<sup>-/-</sup> (red) or *Trex1* WT (blue) mice of indicated *Tcra* or *Ighm* genotype were graded for fibrosis. The average of the two scores was considered the total fibrosis score for each animal.

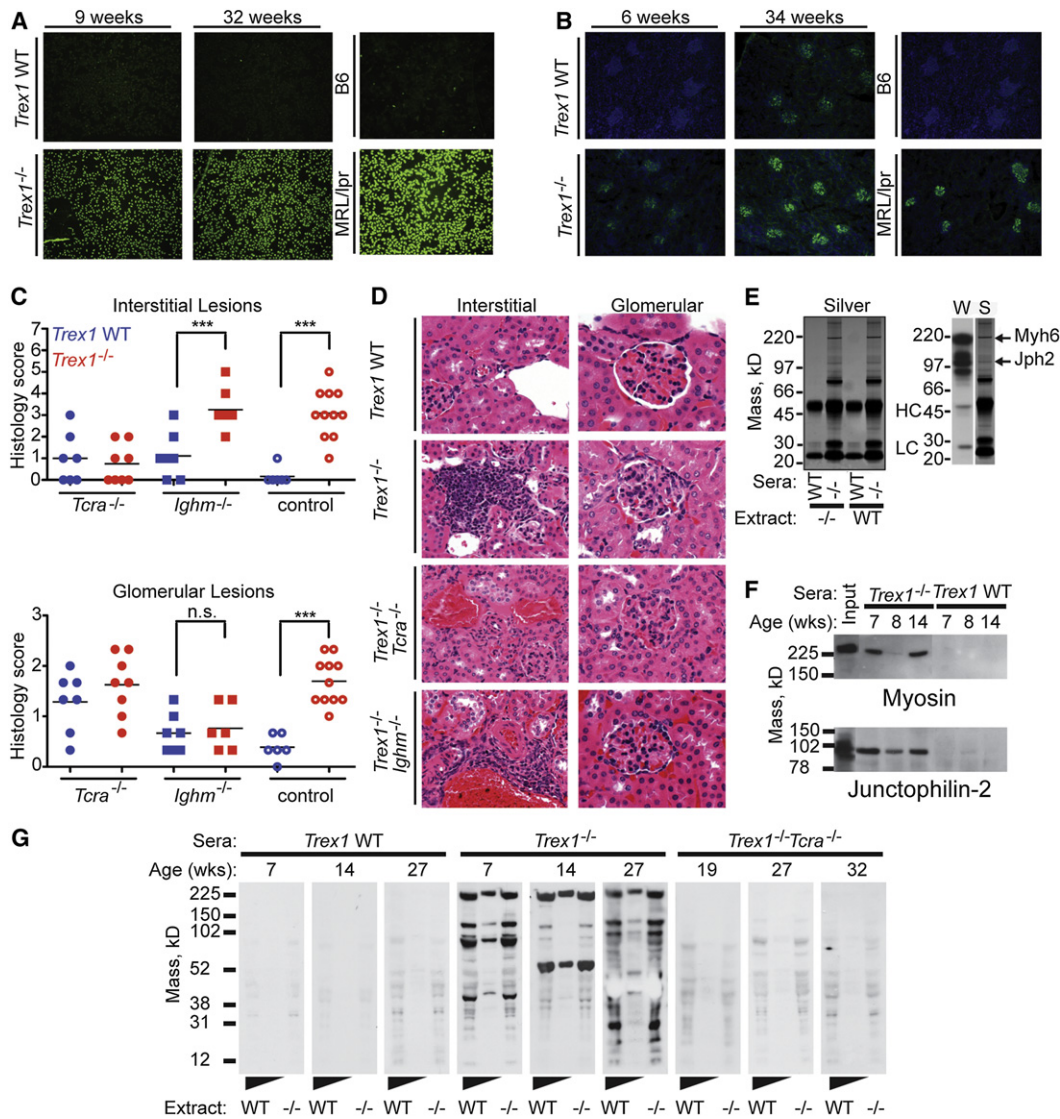


**Figure 6. T Cell-Dependent Autoantibody Specificities in *Trex1*<sup>-/-</sup> Mice**

(A) Antinuclear antibodies in *Trex1* WT (top) or *Trex1*<sup>-/-</sup> (bottom) sera from age-matched mice. Serum from a MRL-*lpr/lpr* mouse served as a positive control. (B) Kidney sections from *Trex1* WT (top) or *Trex1*<sup>-/-</sup> (bottom) were stained with anti-mouse IgG (green) and DAPI (blue). (C) Interstitial kidney inflammation scores (top) and glomerulonephritis scores (bottom) for mice of the indicated genotypes. Each glomerular data point represents the average score of three individual glomeruli per animal. \*\*\**p* ≤ 0.0005. (D) Representative images of interstitial inflammation (left) and individual glomeruli (right) from mice of the indicated genotypes. Note that the cuboidal parietal epithelium of Bowman's capsule is a normal finding in male mice. All images are shown at 600× magnification. (E) Silver stain of heart extract immunoprecipitations, using sera from WT or *Trex1*<sup>-/-</sup> mice. Immunoglobulin heavy chain (HC) and light chain (LC) are indicated. The right panel shows a protein immunoblot (W) of heart extract blotted with *Trex1*<sup>-/-</sup> sera compared to the silver stain (S) of the proteins immunoprecipitated with the same sera. (F) Coimmunoprecipitation of heart extracts with sera from *Trex1*<sup>-/-</sup> or WT mice, immunoblotted with the indicated antibodies. (G) Heart extracts from *Rag2*<sup>-/-</sup> (neat and 1:5 diluted) and *Trex1*<sup>-/-</sup> *Rag2*<sup>-/-</sup> mice blotted with sera from *Trex1* WT, *Trex1*<sup>-/-</sup>, or *Trex1*<sup>-/-</sup> *Tcra*<sup>-/-</sup> mice of indicated ages and detected with HRP-conjugated anti-mouse IgG.

We identify lupus-like features as well as tissue-specific autoantibody responses in *Trex1*<sup>-/-</sup> mice. Together, these findings provide an integrated picture of the development of autoimmune disease caused by *Trex1* deficiency and a framework for understanding its progression, with important implications for the development of therapies for human AGS, which is currently untreatable and incurable.

We propose a model—based on the six genetic crosses that ameliorate disease and our in vivo tracking of the type I IFN response in *Trex1*<sup>-/-</sup> mice—that links chronic activation of the ISD pathway to lymphocyte-dependent autoimmune attack of specific target tissues (Figure S2). First, a geographically restricted subset of nonhematopoietic cells in the target tissue accumulates sufficient endogenous DNA substrates to trigger

a STING- and IRF3-dependent type I IFN response. This response initiates in utero and is reliably detectable in specific tissues within a day after birth, prior to the emergence of mature lymphocytes in mice. Next, the type I IFNs produced by the initiating cells signal to hematopoietic cells and are required to drive a T cell-dependent inflammation and autoantibody response that results in a rapidly progressing autoimmune destruction of the target tissue. Genetic deletion of *Tmem173*, *Irf3*, *Ifnar1*, *Rag2*, *Tcra*, or *Ighm* rescues the mice from mortality at distinct points along this continuum. This model suggests a nonhematopoietic origin of the dysregulated innate immune response that ultimately leads to autoimmunity and reveals how therapies targeted to specific points in this pathway might intercept disease progression. For example, efforts to block the accumulation of Trex1 substrates or inhibit the ISD pathway would act at the earliest phase of the autoimmune disease. In contrast, lymphocyte depletion would potentially and temporarily ameliorate inflammation and tissue damage, but the dysregulated innate immune response would remain.

The application of an in vivo reporter of the IFN response in *Trex1*-deficient mice reveals the initiation of this autoimmune disease with unprecedented temporal and spatial resolution. Perhaps most remarkably, we show that a relatively small number of cells near the endocardial surface generates the earliest detectable IFN response in the heart, raising the important question of what is unique about these cells compared to other cells in the same region. We speculate that these cells are the first to reach a threshold level of accumulated Trex1 DNA substrates that triggers the ISD pathway, and, more broadly, that the specific target organs affected by *Trex1* deficiency reflect specific cell types that trigger the early IFN response within these tissues. We are currently exploring why certain cells initiate early IFN production in the target organs of *Trex1*<sup>-/-</sup> mice, and the ability to isolate and sort these cells based on the fluorescent reporter of type I IFN signaling will allow for a direct comparison of these cells to their uninvolved neighbors within the same tissue.

We show that both T cells and B cells contribute to the autoimmune disease in *Trex1*-deficient mice, but through distinct and genetically separable mechanisms. T cells are necessary and sufficient for the tissue-specific autoimmune inflammation and fibrosis, whereas B cells are not required for either of these key disease features. However, the presence of B cells is associated with a dramatic acceleration of morbidity and mortality in *Trex1*-deficient mice. We found that membranoproliferative glomerulonephritis in *Trex1*-deficient mice uniquely requires B cells, but we find it unlikely that this relatively mild glomerular damage explains the dramatic difference in mortality between plain *Trex1*<sup>-/-</sup> mice and *Trex1*<sup>-/-</sup>*Ighm*<sup>-/-</sup> mice. Importantly, our finding that B cells are dispensable for nearly all of the autoimmune inflammation in *Trex1*-deficient mice may offer a partial explanation for the disappointing results of some of the B cell-targeted therapies that are currently being trialed in SLE patients (Looney, 2010), especially given the strong genetic association of rare *TREX1* mutations with this disease. We suggest that some of the inflammatory processes in a subset of SLE patients might progress in the absence of B cells, particularly in the context of established disease.

How might B cells contribute to disease in *Trex1*-deficient mice? Current models suggest at least three possibilities, all tied to the antigen specificity of the autoreactive B cells: antigen presentation to T cells, pathogenic autoantibodies, and production of proinflammatory cytokines. Because *Trex1*<sup>-/-</sup>*Ighm*<sup>-/-</sup> mice still develop extensive T cell-dependent inflammation and fibrosis, B cells cannot be the major antigen-presenting cells in this disease. Notably, our findings in *Trex1*<sup>-/-</sup> mice differ from those in the MRL-*lpr/lpr* model of murine lupus, in which B cells are prominent antigen-presenting cells and are required for tissue inflammation (Chan and Shlomchik, 1998). Thus, whereas B cells are clearly important in both model systems, the mechanisms by which they contribute to disease may be different and determined by the nature of the genetic predisposition to autoimmunity. We propose that the various (and still poorly understood) genetic contributions to human SLE will also reveal distinct mechanistic contributions of B cells, suggesting that a pharmacogenomics approach to SLE would yield more effective therapies to target these different disease mechanisms.

We identified T cell-dependent autoantibodies that target abundant, tissue-specific autoantigens, suggesting that these autoantibodies might contribute to the rapidly progressing autoimmune pathology in *Trex1*-deficient mice. To further explore this possibility, we injected pooled sera from *Trex1*<sup>-/-</sup> mice into WT recipients twice in 2 days and sacrificed the recipients 5 days after the second injection to look for signs of a type II hypersensitivity response. However, we did not find any evidence for inflammation in WT mice injected with *Trex1*<sup>-/-</sup> sera, suggesting that at least in this acute experimental setting, the autoantibodies do not mediate direct toxicity in an otherwise healthy recipient (data not shown). It remains possible, however, that the autoantibodies directly contribute to disease in the context of chronic, T cell-dependent inflammation. Interestingly, the major heart autoantigens in *Trex1*<sup>-/-</sup> mice are cytosolic proteins, which suggests that exposure of these autoantigens during inflammation-associated cell death in the target tissue might be required to reveal the epitopes detected by the autoreactive B cells. Finally, whether B cells produce relevant proinflammatory cytokines in *Trex1*-deficient mice is currently unknown, but can be explored in detail now that the major heart autoantigen specificities have been identified. Thus, although the precise mechanisms by which B cells contribute to disease will require further study, our findings suggest that B cells may play an important role in AGS and warrant a more thorough search for autoantibody specificities in the human disease.

In summary, we describe the initiation and stepwise development of IFN-dependent autoimmunity in a mouse model of specific human autoimmune diseases. These findings provide detailed insight into how dysregulated activation of cell-intrinsic antiviral sensors leads to autoimmune pathology and suggest new avenues for therapeutic intervention to intercept the disease process.

## EXPERIMENTAL PROCEDURES

### Mice

*Rag2*<sup>-/-</sup>, *Tcra*<sup>-/-</sup>, and *Ighm*<sup>-/-</sup> mice were purchased from Jackson Laboratories. Rosa26-YFP and Mx-Cre mice were generously provided by A. Rudensky

and K. Rajewsky, respectively. *Irfar1*<sup>-/-</sup> CD45.2 mice were kindly provided by M.-K. Kaja. *Trex1*<sup>-/-</sup> mice were generously provided by D. Barnes and T. Lindahl. *Tmem173*<sup>-/-</sup> mice were generated as described (Ishikawa et al., 2009) and backcrossed three times to C57BL/6 before intercrossing with *Trex1*<sup>-/-</sup> mice. *Mavs*<sup>-/-</sup> mice on a C57BL/6 background were generated by M. Loo, M.G., Jr., and colleagues (unpublished data). All mice were maintained and used in a specific-pathogen-free facility at the University of Washington in accordance with the guidelines of the UW Institutional Animal Care and Use Committee.

### Pathology

Tissues were fixed in 10% neutral buffered formalin, paraffin embedded, cut into 5  $\mu$ m sections, and stained with hematoxylin and eosin or picosirius red. All tissues were coded to remove genotype identification and were evaluated for evidence of inflammation, fibrosis, and in some cases mucosal lesions. Numerical scores were assigned based on degree of severity (0 = normal to 5 = most severe) and extent of pathology (E1 = percent of tissue affected in any manner, E2 = percent of tissue affected in most severe manner). Unless otherwise indicated, the sum of individual scores was used to obtain a total tissue histological score. Please see Table S1 for more specific information about the scoring criteria for each tissue.

### Bone Marrow Chimeras and Flow Cytometry

*Rag2*<sup>-/-</sup> or *Trex1*<sup>-/-</sup> *Rag2*<sup>-/-</sup> female mice were irradiated with 800 rads from a cesium source and reconstituted 24 hr later with  $2 \times 10^6$  bone marrow cells. Mice were pretreated with and maintained on antibiotics (neomycin sulfate + polymyxin B) for 3 weeks postreconstitution. After 6–9 weeks, mice were harvested for histology and flow cytometry analysis. Spleens and hearts were treated with collagenase/DNase prior to surface antibody staining with anti-CD4 (GK1.5, BD Biosciences), anti-CD45.1 (A20, eBiosciences), and anti-CD45.2 (104, eBiosciences). Samples were acquired on a FACSCanto (BD Biosciences) and analyzed with FlowJo software (TreeStar).

### Immunofluorescence and ANA/ELISA Assays

For visualization of YFP reporter fluorescence, hearts were fixed in 4% paraformaldehyde overnight, cryoprotected in PBS with 30% sucrose, and frozen in Tissue-Tek OCT embedding compound (Electron Microscopy Sciences). 5  $\mu$ m tissue sections were cut on a Leica CM1900 cryostat (Leica Microsystems) and stained with polyclonal rabbit anti-GFP (Abcam) followed by biotinylated donkey anti-rabbit F(ab')<sub>2</sub> (Jackson ImmunoResearch). YFP signal was further amplified with a FITC-TSA detection kit (Perkin Elmer) according to manufacturer's instructions, and nuclei were counterstained with 4',6-diamidino-2'-phenylindole dihydrochloride (DAPI; Invitrogen). For visualization of immune complex deposition in the kidneys, 5  $\mu$ m sections of fresh frozen tissue were fixed in 100% acetone at -20°C for 10 min and then stained with anti-mouse IgG Alexa Fluor 488 (Invitrogen) and DAPI. Digital images were acquired with a fluorescence microscope equipped with a monochrome digital CCD camera (Orca-ER, Hamamatsu Photonics) and converted to red-blue-green images with Adobe Photoshop CS3 software (Adobe Systems). Detection of anti-nuclear antibodies was performed with 1:200 diluted sera with an ANA (HEp-2) antigen substrate slide kit (MBL-BION) according to manufacturer's instructions. Anti-dsDNA and antichromatin ELISAs were performed as previously described (Martin et al., 2007).

### Quantitative RT-PCR

Embryos were harvested into RNAlater (QIAGEN) and homogenized the next day with a TissueRuptor (QIAGEN) followed by RNA extraction with an RNeasy kit (QIAGEN) according to manufacturer's instructions. Quantitative PCR was performed on a CFX 96 Real-Time System instrument (Biorad). The primers used were ISG15 sense, 5'-GGTGTCCGTGACTAACCAT-3'; ISG15 antisense, 5'-TGGAAAGGGTAAGACCGTCT-3'; HPRT sense, 5'-GTTGGATACA GGCCAGACTTTGTTG-3'; and HPRT antisense, 5'-GAGGGTAGGCTGGCCT ATAGGCT-3'.

### Protein Immunoblots and Coimmunoprecipitation

Heart extracts were prepared and blotted as described previously (Stetson et al., 2008). For coimmunoprecipitations, heart extracts were precleared with Protein G Dynabeads (Invitrogen) and incubated overnight with 1:200

diluted sera from *Trex1*<sup>-/-</sup> or control mice. Immunoprecipitated samples were then captured by Protein G Dynabeads, washed extensively, and uncoupled from the beads by boiling. Samples were separated by SDS-PAGE, transferred to PVDF membranes, and incubated with anti-myosin heavy chain or anti-junctophilin-2 (Santa Cruz Biotechnology), followed by HRP-conjugated secondary antibodies.

### SUPPLEMENTAL INFORMATION

Supplemental Information includes two figures and one table and can be found with this article online at doi:10.1016/j.immuni.2011.11.018.

### ACKNOWLEDGMENTS

We are grateful to D. Barnes and T. Lindahl for providing *Trex1*-deficient mice; to A. Rudensky for Rosa26-YFP reporter mice; to K. Rajewsky for Mx-Cre mice; to M.-K. Kaja for CD45.1 congenic *Irfar1*<sup>-/-</sup> mice; to M. Pric and N. Zhang for help with bone marrow chimeras; to D. Winant and the Stanford PAN facility for mass spec analysis; to B. Johnson for expert histology preparation; to L. Reinhardt for help with immunofluorescence; and to Y. Crow and the D.B.S. lab for helpful discussions. D.B.S. is a scholar of the Rita Allen Foundation. This work was supported by grants from the NIH (A1084914 to D.B.S.; AR48796 to K.B.E.), the European Union (FP7/2007-2013) grant agreement number 241779 (NIMBL: <http://www.NIMBL.eu/ni/home>), and the Lupus Research Institute (all to D.B.S.).

Received: July 5, 2011

Revised: October 17, 2011

Accepted: November 15, 2011

Published online: January 26, 2012

### REFERENCES

- Ablasser, A., Bauernfeind, F., Hartmann, G., Latz, E., Fitzgerald, K.A., and Hornung, V. (2009). RIG-I-dependent sensing of poly(dA:dT) through the induction of an RNA polymerase III-transcribed RNA intermediate. *Nat. Immunol.* 10, 1065–1072.
- Banchereau, J., and Pascual, V. (2006). Type I interferon in systemic lupus erythematosus and other autoimmune diseases. *Immunity* 25, 383–392.
- Barbalat, R., Ewald, S.E., Mouchess, M.L., and Barton, G.M. (2011). Nucleic acid recognition by the innate immune system. *Annu. Rev. Immunol.* 29, 185–214.
- Barrat, F.J., Meeker, T., Gregorio, J., Chan, J.H., Uematsu, S., Akira, S., Chang, B., Duramad, O., and Coffman, R.L. (2005). Nucleic acids of mammalian origin can act as endogenous ligands for Toll-like receptors and may promote systemic lupus erythematosus. *J. Exp. Med.* 202, 1131–1139.
- Barton, G.M., and Kagan, J.C. (2009). A cell biological view of Toll-like receptor function: regulation through compartmentalization. *Nat. Rev. Immunol.* 9, 535–542.
- Chan, O., and Shlomchik, M.J. (1998). A new role for B cells in systemic autoimmunity: B cells promote spontaneous T cell activation in MRL-lpr/lpr mice. *J. Immunol.* 160, 51–59.
- Chiu, Y.H., Macmillan, J.B., and Chen, Z.J. (2009). RNA polymerase III detects cytosolic DNA and induces type I interferons through the RIG-I pathway. *Cell* 138, 576–591.
- Christensen, S.R., Shupe, J., Nickerson, K., Kashgarian, M., Flavell, R.A., and Shlomchik, M.J. (2006). Toll-like receptor 7 and TLR9 dictate autoantibody specificity and have opposing inflammatory and regulatory roles in a murine model of lupus. *Immunity* 25, 417–428.
- Crow, Y.J., Hayward, B.E., Parmar, R., Robins, P., Leitch, A., Ali, M., Black, D.N., van Bokhoven, H., Brunner, H.G., Hamel, B.C., et al. (2006). Mutations in the gene encoding the 3'-5' DNA exonuclease TREX1 cause Aicardi-Goutières syndrome at the AGS1 locus. *Nat. Genet.* 38, 917–920.
- de Vries, B., Steup-Beekman, G.M., Haan, J., Bollen, E.L., Luyendijk, J., Frants, R.R., Terwindt, G.M., van Buchem, M.A., Huizinga, T.W., van den

- Maagdenberg, A.M., and Ferrari, M.D. (2010). TREX1 gene variant in neuropsychiatric systemic lupus erythematosus. *Ann. Rheum. Dis.* 69, 1886–1887.
- Harley, I.T., Kaufman, K.M., Langefeld, C.D., Harley, J.B., and Kelly, J.A. (2009). Genetic susceptibility to SLE: new insights from fine mapping and genome-wide association studies. *Nat. Rev. Genet.* 10, 285–290.
- Ishii, K.J., Coban, C., Kato, H., Takahashi, K., Torii, Y., Takeshita, F., Ludwig, H., Sutter, G., Suzuki, K., Hemmi, H., et al. (2006). A Toll-like receptor-independent antiviral response induced by double-stranded B-form DNA. *Nat. Immunol.* 7, 40–48.
- Ishikawa, H., Ma, Z., and Barber, G.N. (2009). STING regulates intracellular DNA-mediated, type I interferon-dependent innate immunity. *Nature* 461, 788–792.
- Jin, L., Xu, L.G., Yang, I.V., Davidson, E.J., Schwartz, D.A., Wurfel, M.M., and Cambier, J.C. (2011). Identification and characterization of a loss-of-function human MPYS variant. *Genes Immun.* 12, 263–269.
- Kolumam, G.A., Thomas, S., Thompson, L.J., Sprent, J., and Murali-Krishna, K. (2005). Type I interferons act directly on CD8 T cells to allow clonal expansion and memory formation in response to viral infection. *J. Exp. Med.* 202, 637–650.
- Kühn, R., Schwenk, F., Aguet, M., and Rajewsky, K. (1995). Inducible gene targeting in mice. *Science* 269, 1427–1429.
- Lande, R., Gregorio, J., Facchinetti, V., Chatterjee, B., Wang, Y.H., Homey, B., Cao, W., Wang, Y.H., Su, B., Nestle, F.O., et al. (2007). Plasmacytoid dendritic cells sense self-DNA coupled with antimicrobial peptide. *Nature* 449, 564–569.
- Leadbetter, E.A., Rifkin, I.R., Hohlbaum, A.M., Beaudette, B.C., Shlomchik, M.J., and Marshak-Rothstein, A. (2002). Chromatin-IgG complexes activate B cells by dual engagement of IgM and Toll-like receptors. *Nature* 416, 603–607.
- Lebon, P., Badoual, J., Ponsot, G., Goutières, F., Hémeury-Cukier, F., and Aicardi, J. (1988). Intrathecal synthesis of interferon-alpha in infants with progressive familial encephalopathy. *J. Neurol. Sci.* 84, 201–208.
- Lee-Kirsch, M.A., Gong, M., Chowdhury, D., Senenko, L., Engel, K., Lee, Y.A., de Silva, U., Bailey, S.L., Witte, T., Vyse, T.J., et al. (2007). Mutations in the gene encoding the 3'-5' DNA exonuclease TREX1 are associated with systemic lupus erythematosus. *Nat. Genet.* 39, 1065–1067.
- Looney, R.J. (2010). B cell-targeted therapies for systemic lupus erythematosus: an update on clinical trial data. *Drugs* 70, 529–540.
- Martin, D.A., Zhang, K., Kenkel, J., Hughes, G., Clark, E., Davidson, A., and Elkon, K.B. (2007). Autoimmunity stimulated by adoptively transferred dendritic cells is initiated by both alphabeta and gammadelta T cells but does not require MyD88 signaling. *J. Immunol.* 179, 5819–5828.
- Morita, M., Stamp, G., Robins, P., Dulic, A., Rosewell, I., Hrivnak, G., Daly, G., Lindahl, T., and Barnes, D.E. (2004). Gene-targeted mice lacking the Trex1 (DNase III) 3'→5' DNA exonuclease develop inflammatory myocarditis. *Mol. Cell. Biol.* 24, 6719–6727.
- Nagata, S., Hanayama, R., and Kawane, K. (2010). Autoimmunity and the clearance of dead cells. *Cell* 140, 619–630.
- Namjou, B., Kothari, P.H., Kelly, J.A., Glenn, S.B., Ojwang, J.O., Adler, A., Alarcón-Riquelme, M.E., Gallant, C.J., Boackle, S.A., Criswell, L.A., et al. (2011). Evaluation of the TREX1 gene in a large multi-ancestral lupus cohort. *Genes Immun.* 12, 270–279.
- Rice, G., Newman, W.G., Dean, J., Patrick, T., Parmar, R., Flintoff, K., Robins, P., Harvey, S., Hollis, T., O'Hara, A., et al. (2007a). Heterozygous mutations in TREX1 cause familial chilblain lupus and dominant Aicardi-Goutieres syndrome. *Am. J. Hum. Genet.* 80, 811–815.
- Rice, G., Patrick, T., Parmar, R., Taylor, C.F., Aeby, A., Aicardi, J., Artuch, R., Montalto, S.A., Bacino, C.A., Barroso, B., et al. (2007b). Clinical and molecular phenotype of Aicardi-Goutieres syndrome. *Am. J. Hum. Genet.* 81, 713–725.
- Srinivas, S., Watanabe, T., Lin, C.S., William, C.M., Tanabe, Y., Jessell, T.M., and Costantini, F. (2001). Cre reporter strains produced by targeted insertion of EYFP and ECFP into the ROSA26 locus. *BMC Dev. Biol.* 1, 4.
- Stark, G.R., Kerr, I.M., Williams, B.R., Silverman, R.H., and Schreiber, R.D. (1998). How cells respond to interferons. *Annu. Rev. Biochem.* 67, 227–264.
- Stetson, D.B., and Medzhitov, R. (2006a). Recognition of cytosolic DNA activates an IRF3-dependent innate immune response. *Immunity* 24, 93–103.
- Stetson, D.B., and Medzhitov, R. (2006b). Type I interferons in host defense. *Immunity* 25, 373–381.
- Stetson, D.B., Ko, J.S., Heidmann, T., and Medzhitov, R. (2008). Trex1 prevents cell-intrinsic initiation of autoimmunity. *Cell* 134, 587–598.
- Takahashi, I., Iijima, H., Katashima, R., Itakura, M., and Kiyono, H. (1999). Clonal expansion of CD4+ TCRbeta+ T cells in TCR alpha-chain-deficient mice by gut-derived antigens. *J. Immunol.* 162, 1843–1850.
- Theofilopoulos, A.N., Baccala, R., Beutler, B., and Kono, D.H. (2005). Type I interferons (alpha/beta) in immunity and autoimmunity. *Annu. Rev. Immunol.* 23, 307–336.
- Yan, N., Regalado-Magdos, A.D., Stiggelbout, B., Lee-Kirsch, M.A., and Lieberman, J. (2010). The cytosolic exonuclease TREX1 inhibits the innate immune response to human immunodeficiency virus type 1. *Nat. Immunol.* 11, 1005–1013.
- Yang, Y.G., Lindahl, T., and Barnes, D.E. (2007). Trex1 exonuclease degrades ssDNA to prevent chronic checkpoint activation and autoimmune disease. *Cell* 131, 873–886.